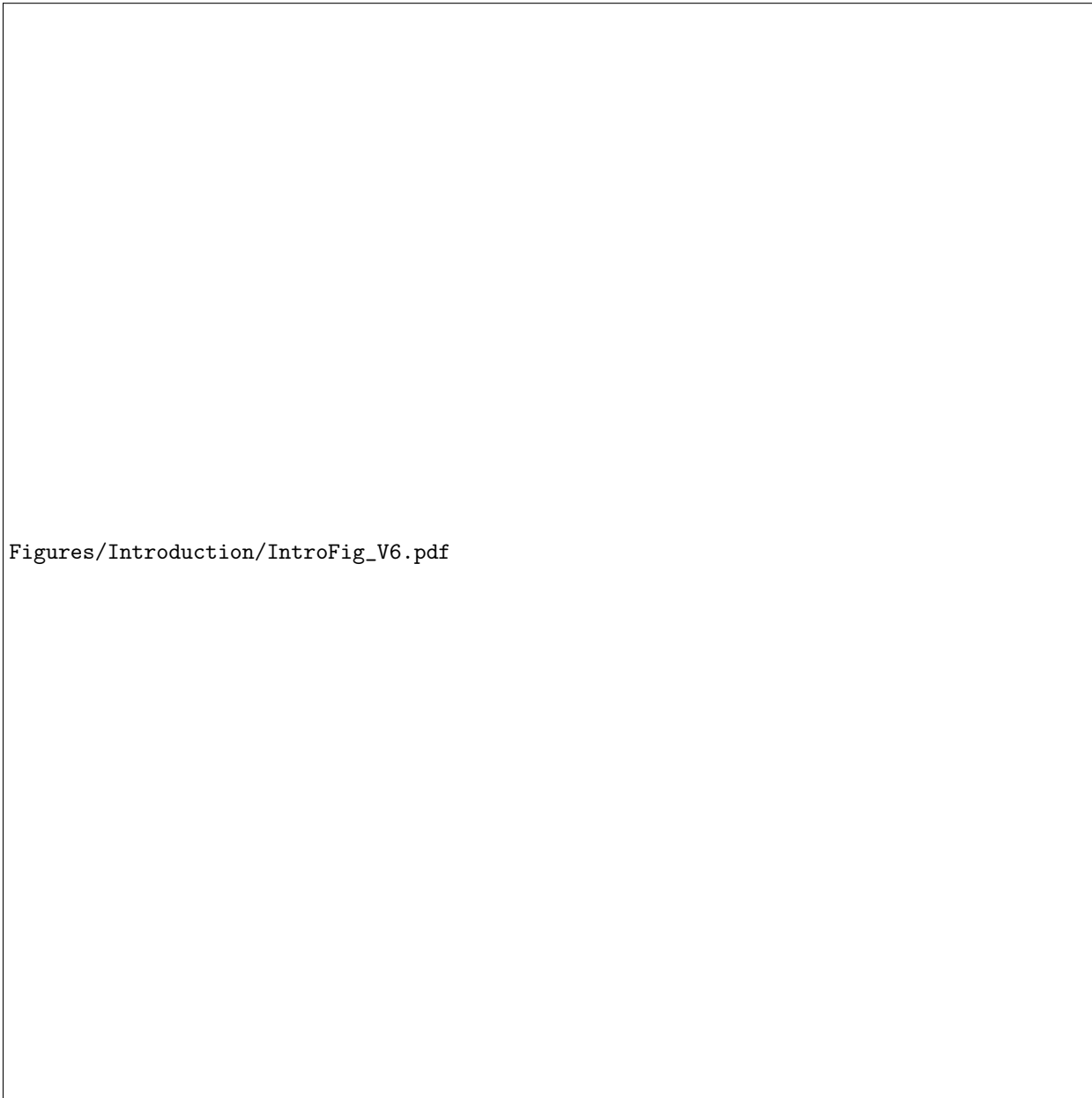


Understanding the origin of toughness enhancement in complex architected ceramic composites by developing and using an anisotropic variational fracture theory

1 Introduction

Research objective (Ro): *This project seeks to derive fundamental scientific knowledge of how architectural motifs in 3D ceramic composites dictate their toughness and damage tolerance.*

In most engineering materials, from steels to ceramics, strength and toughness are mutually exclusive. That



Figures/Introduction/IntroFig_V6.pdf

Figure 1: The complex architecture of SBs and ceramic composites. (a) Cylindrical, concentric layers of silica in the spicules of the marine sponge *Euplectella aspergillum* (modified from [?]). (b) Brick-and-mortar architecture of calcium carbonate tablets in nacre (molluscan shell) (reprinted from [?]). (c) A SiC/graphite composite made using fibrous monolith construction techniques (reprinted from [?]). {f:intro}

is, there are few materials that are both strong and tough [?]. This is a critical bottleneck for aerospace, transportation, and energy production technologies. A very interesting class of materials that could provide strategies for resolving this bottle neck are Structural Bio-materials (Fig. 1), such as bone and shell. While Structural Bio-materials (SBs) are often composed of >95% brittle ceramic material by volume, they have been shown to possess extraordinary toughness and damage tolerance properties while being able to maintain both strength and stiffness [? ? ? ?]. For example, the total energy dissipated during the fracture of nacre has been shown to exceed that of its constituent ceramic material, aragonite, by three orders of magnitude [? ?]. This is a very intriguing effect since it cannot be explained using standard composite mechanics ideas, such as the rule of mixtures (see Figure 2 (c)) [?]. The key to SBs' remarkable toughness and damage tolerance is believed to be their small-scale complex architecture (Fig. 1 (a)–(b)).

Structural biomaterials are composites, and consist of a ceramic and an organic phase mixed together in intricate 3D patterns over a range of length scales [? ?]. The way that these two phases are interlaced, which we refer to as the SB's architecture, is extremely complex compared to architectures typically seen in engineering composites, such as ceramic matrix composites [? ?]. However, currently there are no mechanics of materials theories that can provide the fundamental scientific knowledge of how different complex architectural motifs, such as those found in SBs, affect a composite's large scale toughness. For example currently there are no mechanics of materials theories that can provide either analytical or numerical solutions that can help us answer questions such as (Q.1) Given a mechanical loading program and mechanical properties of the constituent materials and interfaces in a SB type composite, which architectural motifs are the best for enhancing its toughness? (Q.2) In a SB type composite are the mechanical properties of the interfaces actually more important than the architectural motifs? (Q.3) What are the upper bounds to the potential toughness enhancements that architectural motifs can lead to? (Q.4) Is it critical that the architectural motifs be spread over several length scales, i.e., is hierarchy always important?

Lack of the fundamental scientific knowledge of how small-scale architectural motifs are connected to large scale toughness in SBs, and SB inspired composites, is the key hurdle that is stopping the translation of the remarkable toughness enhancement seen in SBs to engineering materials. The project's research objective is motivated by the need to fill this gap in scientific knowledge.

1.1 Research Strategy (Rs):

We will develop a new mechanics of materials theory—anisotropic variational fracture theory—that will enable accurate numerical simulations of the evolution of complex crack networks in SB type composites and use them to pursue the project's research objective

This research strategy derives from the following *Research hypothesis*, on which the project is based, and the rationale that follows it.

1.2 Research hypothesis (Rh):

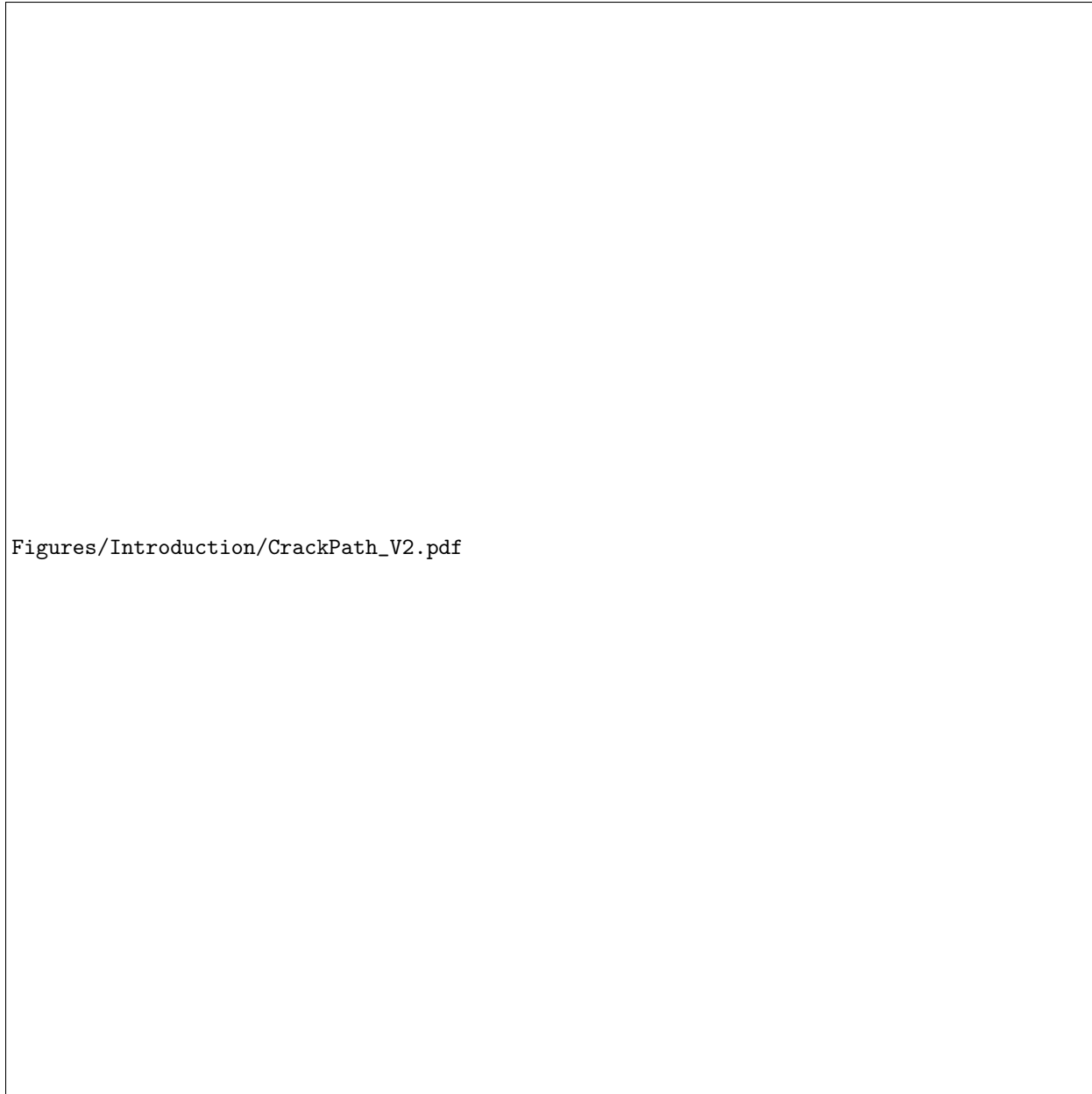
We hypothesize that the toughness enhancement in SB type composites is primarily due to the interfaces within them acting as traps and mazes. The stiff phases fail through brittle fracture. However, the interfaces trap the cracks and make them consume much more energy to spread across the specimen. They do this primarily by pinning, deflecting, and splitting the cracks (see, e.g., Figs. 2(a)–(b) and 4(a)) [? ? ?].

{s:hyp}

The project's hypothesis is based on the Cook-Gordon mechanism [?], which discusses how a weak interface can act as a trap for a crack that is approaching it perpendicularly. The Cook-Gordon mechanism is shown schematically in Figs. 3 (i)–(ii). The hypothesis is supported by experimental observations of dense crack patterns in failed SB type composites [? ?], the PI's previous research on contact interface toughening caused by surface architectures [? ?], and the preliminary results that we discuss in §2.1.

1.3 Rationale underlying our research strategy

The importance of the project's research objective is well acknowledged by the mechanics of materials community. This is evidenced by the phlethora of models that have been put forward in literature for explaining the origin of toughness in SB type composites. The proliferation of the different models is, however, also a reflection of the complexity of the architectural motifs seen in SBs and the complexity of the mechanisms



Figures/Introduction/CrackPath_V2.pdf

Figure 2: Complex crack paths in ceramic composites are responsible for toughness enhancement. (a) Cracks are deflected and split by the concentric layered architecture of a *Monorhaphis Chuni* spicule (reprinted from [?]). (b) Crack splitting and tablet pull-out observed during the fracture of nacre loaded in uniaxial tension (reprinted from [?]). (c) Comparison of toughness of both nacre and SB-inspired layered ceramic composites with their brittle constituents showing a toughness enhancement in excess of what is predicted by the rule of mixtures (reprinted from [?]). {f:hyp}

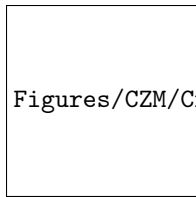
that underlie the SBs' toughness. Architectures of important SBs, such as bone and conch shell (*strombus gigas*), possess at least several dozen architectural parameters. Due to this complexity, it is seldom clear which features are important and should therefore be included in a model. Typical models aimed at explaining toughness enhancement focus on a small subset of the SBs' architectural motifs and also make a number of simplifying assumptions regarding the deformation behavior of the materials and the interfaces. Naturally, by focusing on different architectural subsets and using different simplifying assumptions one can come up with a number of models. For example, there are over five models that are actively discussed in the community for explaining the toughness enhancement in nacre [? ? ? ? ?].

CZM (Hillerborg et al.)	CZM (Xu and Needleman)	Damage me- chanics	Element Deletion	XFEM	RVFT
1. Capable of capturing topology changes independently, i.e., without a priori knowledge of crack path(s), user input, or resorting to ad-hoc, or heuristic techniques.					
No [?]	Yes [? ?]	Yes [?]	Yes	No [? ?]	Yes [?], our Preliminary research, e.g., see Figs. 4, 10
2. Good accuracy. That is, able to quantitatively reproduce experimental observations of growth of cracks and the evolution of a crack network as long as there are no topology changes in the network .)					
-	No [? ? ?]	No	No [?]	competitive	competitive (our Preliminary research, e.g., see Fig. 4, 6)
3. Well conditioned, i.e., no problems with numerically stability.					
Yes	Yes	No	Yes	No [?]	Yes [?], our Preliminary research
4. Mesh independence.					
No	No [? ?]	No	No [?]	Yes [?]	Yes [? ? ?], our Preliminary research
5. Computationally affordable.					
Yes	Yes	No	Yes	Yes	No

Table 1: A comparison of different computational fracture mechanics methods, w.r.t. criteria that are important for pursuing the project's research objective

Many of the models that have been put forward for explaining the toughness enhancement in SBs have their origin in older models that were created for explaining the toughness enhancement in the early generation of engineering composites. Notably, Evans and co-workers [?] put forward a large number of models, which they categorized into “intrinsic” and “extrinsic” toughnening mechanisms, for explaining toughening in ceramic matrix composites. The shear-lag model is another important model, initially put forward by Cox [?], which is widely adapted for explaining the mechanical behavior of SBs. It is quite unlikely that the models based on older models of engineering composites are sufficient for quantitatively capturing the toughness enhancement in SBs. This is because none of those older models incorporate the evolution of complex crack networks and their interaction with 3D interfaces; whereas, as we discussed in section 1.2, there is substantial evidence to suggest that the evolution of complicated crack patterns and their interaction with the SBs architectures is key to the SBs remarkable toughness enhancement. Therefore, any model that aims to quantitatively capture how small-scale architectural motifs dictate large scale toughness needs to incorporate, even, at least in some approximate manner, the evolution of crack patterns.

It is not surprising that previous models do not explicitly model the evolution of crack patterns in SBs. Since, even with state of the art computational fracture mechanics techniques it is quite challenging to accurately simulate the evolution of complex crack patterns in SB type composites, let alone capture their interaction with the SBs' 3D interfaces. We studied a number of the most widely used computational fracture mechanics techniques with regard to their suitability for pursuing the project's research objective. We evaluated the different techniques using five criteria that we deemed to be most important for the project's success. Our evaluation is summarized in Table. 1. Among the different methods, the generalized Cohesive Zone (CZ) methods, the extended finite element method (XFEM) and the regularized, variational fracture theory



Figures/CZM/CrackPathTopology_V1.pdf

Figure 3:

{f:topchanges}

(RVFT) based methods came closest to satisfying the criteria. However, we found that none of them can readily be applied for pursuing the project's research objective. They all need further development in one or more aspects. For example, we found that the generalized CZ method is not very accurate in reproducing experimentally observed crack paths [? ? ?]. Its predicted crack paths are also highly mesh sensitive. The XFEM is unsuitable for this project since it can not independently handle topology changes during the evolution of crack patterns. That is, it cannot be used to capture phenomena such as the merging of two (or more) cracks to form a single crack (Figure 3(a).i–ii), the splitting of a crack into two (or more) daughter branches (Figure 3(b).i–iii), and the nucleation of new cracks (Figure 3(c).i–iii). For further elaboration on why the generalized CZ methods and the XFEM are unsuitable for pursuing the research objective please see §A.1.

The primary drawback of the RVFT is its computationally expense. Through our preliminary research we found that the RVFT's computationally expense is intimately connected to a feature of the theory that we call "broadening". We explain this feature in §3.2. Also through our preliminary research, we have found a highly promising strategy for alleviating broadening and making the RVFT ideally suitable for pursuing the research objective. We discuss this strategy in §3.2. On the other hand, we did not come across any strategies for alleviating the drawbacks of the generalized CZ and XFEM methods which fit into the three year time frame of the project. Therefore, through this project we propose to develop the RVFT by alleviating the problem of broadening, and demonstrate the capability of the resulting theory in helping us achieve the project's overarching research objective.

We call the theory that will result from us carrying out the proposed research program the anisotropic RVFT or aRVFT. We discuss the theoretical solid mechanics research that we will carry out to alleviate *broadening* and build the aRVFT in §4.1. We discuss the experimental mechanics research that we will carry out to demonstrate the aRVFT's capability in §4.2. The problem of broadening and our proposed resolution of it are both intimately related to the technical details of the RVFT. Therefore, we begin by first giving a brief technical overview of the RVFT.

2 Previous and current work that motivates our hypothesis

{s:prevcurr}

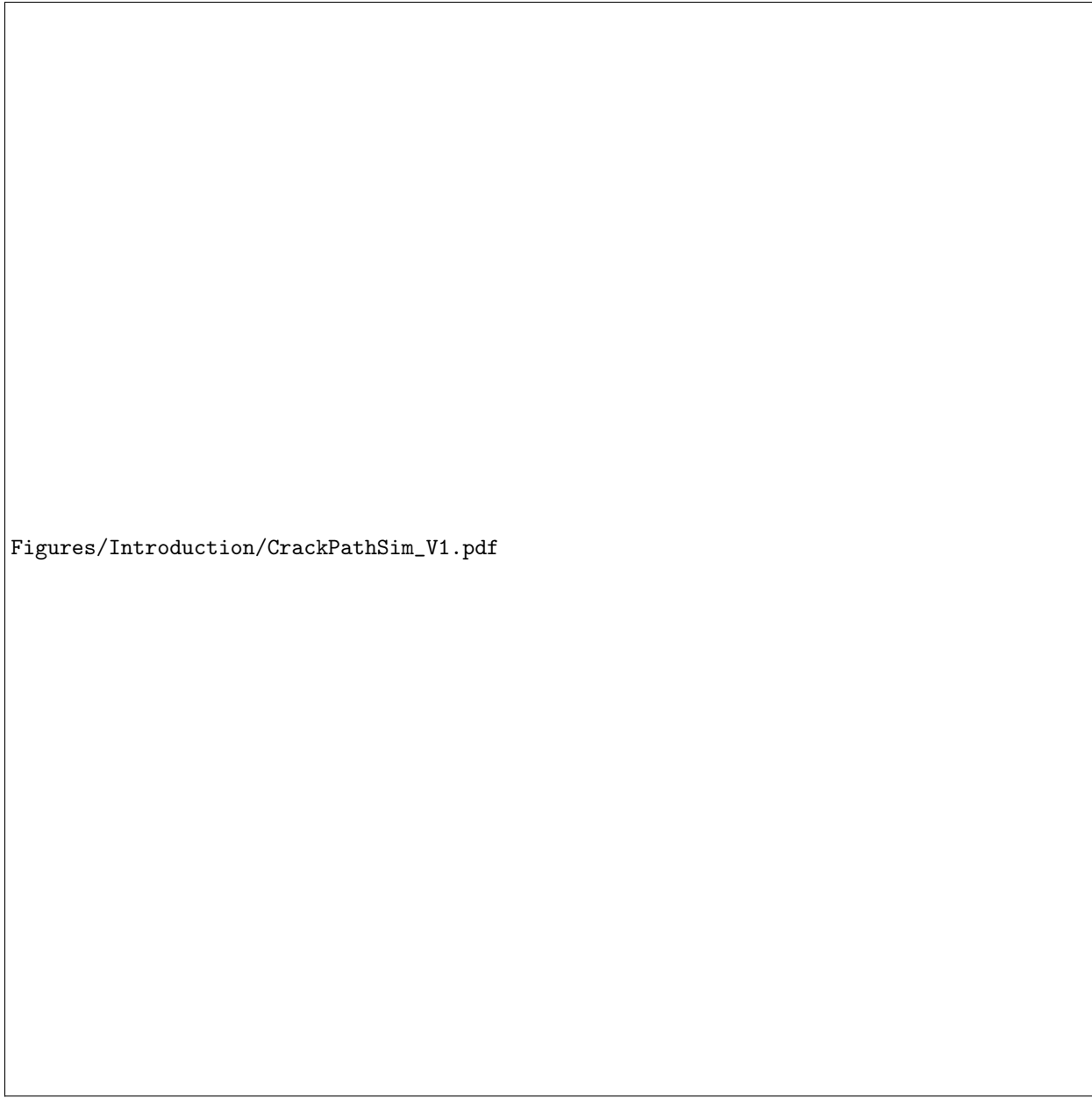
2.1 Preliminary Results

{s:curr}

One of the primary differences between the wavy surface adhesion and wavy interface fracture problems is that in the case of fracture, a crack is not required to travel along the interface as it is in the adhesion problem. Rather, in the fracture problem, the crack can either travel along the interface or propagate through the bulk (see Figure 5 (c)). The RVFT tool is ideally suited to handle this additional level of complexity.

As preliminary research, we implemented non-linear finite element techniques [?] to numerically solve the RVFT Eqns. (??) using the algorithms presented in [?]. The results of these calculations are shown in Figures 6–5. These results were generated for the special case of small deformations and Ψ_0 corresponding to the strain energy density of a homogeneous, isotropic, linear elastic material model. We found that in many important cases the results of the RVFT match the predictions of linear elastic fracture mechanics (LEFM), see, e.g., Figure 6 (a). It has also been shown that the crack path predicted by the RVFT matches the crack path seen in many experiments [? ? ?]. We were also able to reproduce these results, e.g., see Figure 6 (b).

The PI then performed a preliminary study of crack propagation in materials with wavy interfaces using the RVFT tool (see Figure 5 (b)–(e)). In these simulations we allowed g_c to vary spatially, so that in most of



Figures/Introduction/CrackPathSim_V1.pdf

Figure 4: Initial RVFT results show accurate predictions of crack paths and capture toughening mechanisms such as crack deflection in 2D composites. (a) The convoluted crack path in a 2D layered SiC/graphite composite loaded in three point bending. (b) The load-displacement response of the SiC/graphite composite. (a), and (b) are reprinted from [?]. (c) Crack path predicted by the RVFT tool for a model of the composite shown in (a). (d) The load-displacement response obtained from the RVFT tool predictions for different numbers of layers.

{f:sim}

the solid it had a high value, g_b , and at a predefined wavy interface of finite thickness, it had a low value, g_I . In our preliminary simulations depending on the parameters A/λ and g_I/g_b the failure of the interface displayed very rich mechanics. Here, A and λ are the amplitude and the wavelength of the interface, respectively. For example, we found that at small A/λ the crack always propagated along the interface (see Figure 5 (c)). However, at larger A/λ the crack repeatedly ventured out of the interface into the bulk and then back into the interface through a series of energy dissipating instabilities, see Figure 5 (c). The instabilities occurring during the crack propagation are identified and shown in Figure 5 (d)–(e). This led to substantial toughening in the load-displacement response—i.e., area under the load-displacement curve

(see Figure 5 (b)). Namely, the peak load is increased by 6.8% and the fracture toughness is enhanced by 55.3%.

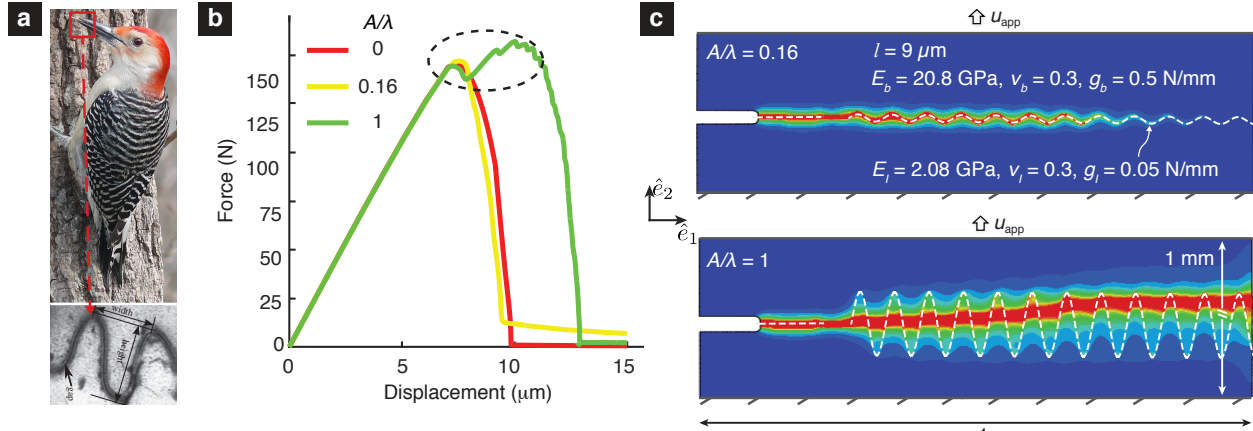


Figure 5: (a) Wavy interfaces between keratin scales in the beak of the red bellied woodpecker (photo from [?], micrograph reprinted from [?]). (b) Load–displacement curves for different aspect ratios A/λ of the interface shown in (c). (c) Crack propagation along a wavy interface for $A/\lambda = 0.16$ and 1 , respectively. The interface is shown as a dashed line. (d) Zoom-in view of the load-displacement curve indicated by dashed circle in (b) showing the instabilities during the crack propagation. (e) Snapshots at instability points as indicated in (d).

{f:VFTprelimr}

These examples reveal two interface toughening mechanisms: instabilities induced by the unstable crack propagation through bulk material, and the nucleation of daughter crack ahead of the primary crack. These mechanisms cannot be captured by the CZM and XFEM simulations. The preliminary results suggest that the RVFM is a powerful approach through which we can investigate toughening mechanisms in materials with complex, 3D interfaces.

3 Technical background

3.1 Technical details of RVFT

A crack by definition has zero thickness in the reference configuration. Almost all continuum mechanics fracture theories model cracks as curves or surfaces in the reference configuration. Similarly, some of the most important computational fracture mechanics models, such as XFEM and CZ methods, also model cracks as having zero thickness [? ?]. In contrast, a very conspicuous feature of the RVFT is that in it the crack thickness is non-zero. The crack networks in RVFT are represented using a scalar valued field called the damage or phase field. We denote the damage field as $d(\mathbf{X})$, where \mathbf{X} is a material point in the solid's reference configuration \mathcal{B}_0 . The damage parameter d takes values between zero and unity. By construction, as d increases the material's capacity to store elastic energy degrades. Therefore, d can be interpreted as a measure of damage. When $d = 0$ the material point is completely undamaged, and when $d = 1$ the material point has lost all capacity to store strain energy. (The RVFT, despite a few similarities, is quite different from what are termed *Damage Mechanics* theories.) The crack pattern is the region Ω_c , which is defined to be a path connected subset of the solid \mathcal{B}_0 such that $d(\mathbf{X}) \geq c$, $\forall \mathbf{X} \in \Omega_c$, where c is a real number just smaller than unity, and the set $\{\mathbf{x} \in \Omega_c : d(\mathbf{X}) = 1\}$ is non-empty.

In the following exposition, for the sake of brevity, we will focus on the RVFT version presented by Bourdin et al. [? ?]. That is, we do not discuss the more sophisticated versions of RVFT that include modifications aimed at allaying unrealistic effects, such as fracture during compressive loading and the healing of cracks. However, the preliminary results that we presented in Figs. 6, 5,4 were produced using the version presented by Miehe [?], which is one such sophisticated RVFT version.

The physics underlying Bourdin et al.'s RVFT is the variational fracture theory (VFT) put forward by Marigo and Francfort [?]. The VFT is a generalization of the configurational force balance ideas of Griffith [?]. Griffith postulated that for a crack to grow the energy release rate should equal or exceed the material's fracture toughness. In RVFT this postulate is generalized by requiring that the damage field only grow

{s:proper}

{sec:Technical}

such that the mechanical energy released is greater than or equal to the energy consumed by the fracture processes. For the case of no body forces and surface tractions, this postulate implies that

$$d := \operatorname{Arg} \inf_d g_c/2 \int_{\mathcal{B}_0} (d(\mathbf{X})^2/\ell + \ell \|\nabla_0 d(\mathbf{X})\|^2) d\Omega - \int_{\mathcal{B}_0} \Psi_d(\mathbf{X}, \mathbf{C}, d), d\Omega, \quad (1) \quad \text{f eq:PFT-Funct}$$

subject to the constraint that d at any material point only increase with time. This constraint introduces irreversibility and history dependence into the problem. In (1), the parameter g_c is a measure of the material's fracture toughness, $\|\cdot\|$ is the Euclidean 2-norm, the parameter ℓ has units of length and is called the regularization parameter, $\Psi_d(\mathbf{X}, \mathbf{C}, d) := (1-d)^2 \Psi_0(\mathbf{X}, \mathbf{C})$ is called the degraded strain energy density, where Ψ_0 is the strain energy density of the solid when we ignore all dissipative processes. The tensor $\mathbf{C} := \mathbf{F}^T \mathbf{F}$ is the right Cauchy-Green deformation tensor, where $\mathbf{F} = \nabla_0 \mathbf{u} + \mathbf{I}$ is the deformation gradient, \mathbf{u} is the equilibrium displacement vector, \mathbf{I} is the identity tensor, and $\nabla_0(\cdot)$ is the gradient operator defined with respect to \mathbf{X} . By the equilibrium displacement vector we mean that \mathbf{u} satisfies the dirichlet boundary conditions and the equilibrium equation $\nabla_0 \cdot \mathbf{P} = 0$ on \mathcal{B}_0 , where \mathbf{P} is the first Piola-Kirchhoff stress tensor.

As preliminary research, we implemented non-linear finite element techniques [?] to numerically solve the variational problem posed in (1) using the algorithms presented in [?]. The results of these calculations are shown in Figures 4, 5, 6, and 10. These results were generated for the special case of small deformations and Ψ_0 corresponding to the strain energy density of a isotropic, linear elastic solid. We found that in many important cases the results of the RVFT match the predictions of linear elastic fracture mechanics (LEFM), see, e.g., Figure 6(a). It has been shown that in many cases the crack paths predicted by RVFT match experimentally observed crack paths [? ? ?]. We too saw similar match between RVFT's predictions and experimental observations in our preliminary research, e.g., see Figs. 4, 6(b), and 10.

3.2 Technical problem statement: the problem of “Broadening”

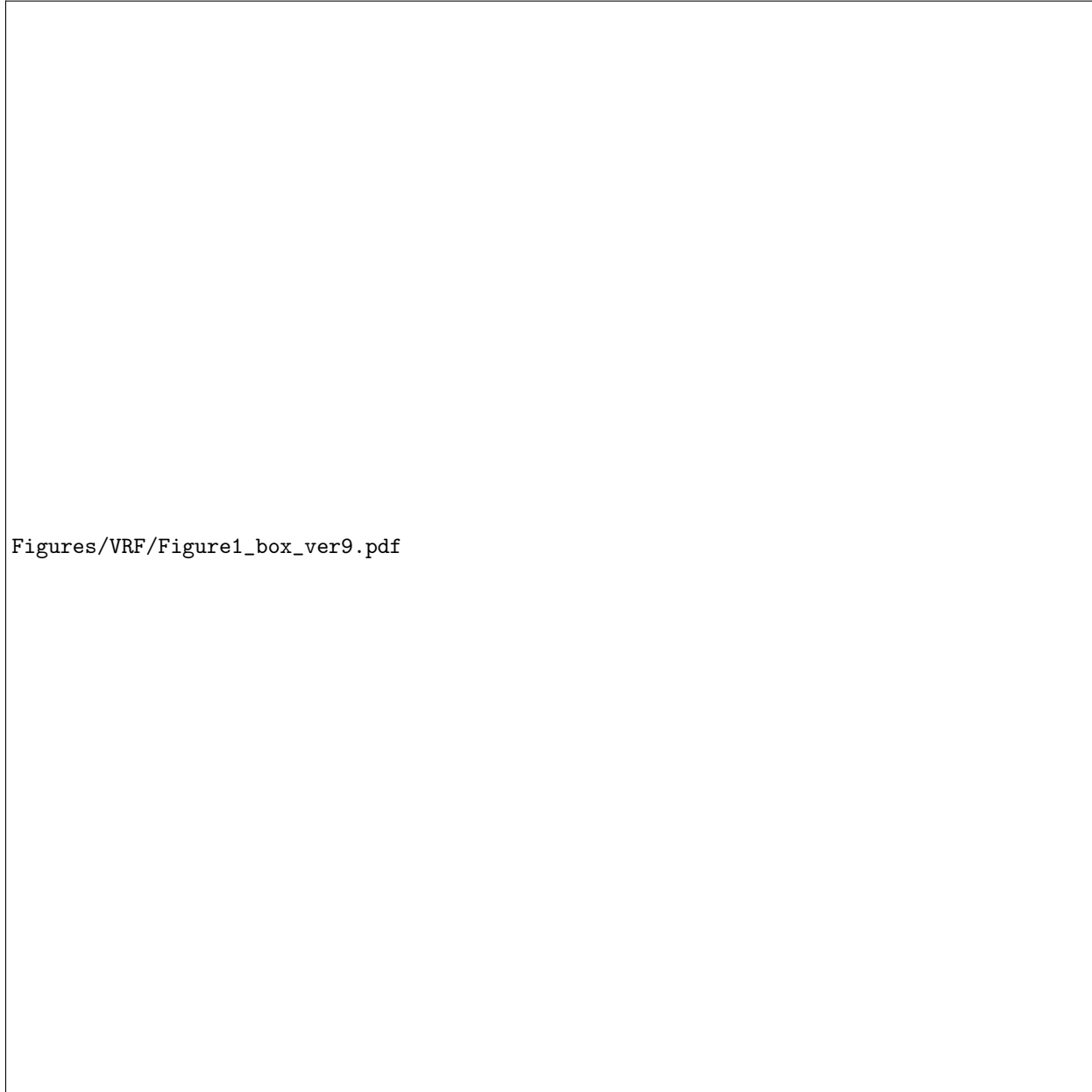
Recall from §3.1 that in RVFT the crack pattern is defined to be the region Ω_c , which has the same dimensionality as the solid \mathcal{B}_0 . That is, cracks in RVFT have finite thickness. This, however, does not preclude RVFT from being a useful and predictive theory of fracture. For instance, consider again the remarkable match of the RVFT's predictions with LEFM and experimental results shown in Figs. 4, 6, and 10. However, for the cracks in the RVFT to be physically meaningful it is important that their thicknesses be much smaller than the physical dimensions of the solid. This is because in the RVFT the crack region Ω_c has zero stiffness. Thus, if a crack thickness is not much smaller than the solid's dimensions then the situation resembles that of a solid undergoing plastic failure rather than brittle fracture. It is generally argued that the thickness of the crack is of the orde of ℓ , the regularization parameter [?]. And hence by choosing ℓ to be much smaller than the characteristic dimension of the solid, W , i.e., $\ell/W \ll 1$, one can ensure that the results are always meaningful, i.e., the failure has the physical features of brittle fracture. However, in some test cases we observed that the crack thickness was comparable to the dimensions of the solid even though ℓ was much smaller than the solid's dimensions. We termed this effect *broadening*. Example test cases displaying broadening are shown in Figure 7.

We found that the broadening effect was not due to human errors or numerical artifacts, but due to the inadequacy of the condition $\ell/W \ll 1$. This fact is best illustrated by the following analytical solution to the variational problem (1) for a simple test case.

Consider a 2D strip of infinite length and width $2W$ that is shown in Figure 7 (d). The strip is composed of an incompressible neo-Hookean material so that the degraded strain energy density in this case is $(1-d)^2(\mu/2)(\lambda_1^2 + \lambda_2^2 - 2)$. The strip has a pre-existing crack along its length (shown in red in Figure 7 (d)). Starting from this state, the strip is uniformly stretched with a stretch ratio of λ_2 in the crack direction (marked as $\hat{\mathbf{e}}_2$ in Figure 7 (d)). Let $\tilde{\beta} := \mu(\lambda_2^2 + 1/\lambda_2^2 - 2)W^2/g_c\ell$ be a dimensionless measure of this straining, where μ is the shear modulus, and let $\tilde{\alpha} := \tilde{\beta} + 1/\tilde{\ell}^2$, where $\tilde{\ell} := \ell/W$. Assuming that the solution does not vary along the strip's length, an analytical solution for the damage field can be obtained for this problem. It can be shown using the analytical solution that in the majority of the strip the damage variable is approximately equal to $\tilde{\beta}/\tilde{\alpha}$, see Figure 7 (g). If $\tilde{\beta}/\tilde{\alpha}$ becomes greater than c , which, recall, is the parameter used for defining the crack region Ω_c , then the crack width will become equal to the strip's width. That is, there will be broadening. And this would occur irrespective of how small $\tilde{\ell}$ is as long as $\tilde{\beta}/\tilde{\alpha}$ is greater than

c , see Figure 7 (g). Therefore in order to prevent broadening, it is also necessary that $\tilde{\beta}/\tilde{\alpha}$ is much smaller than unity, which in terms of dimensional variables reads $\ell \ll \ell_c$, where $\ell_c := g_c/\mu(\lambda_2^2 + 1/\lambda_2^2 - 2)$ is a length scale characteristic of the material and loading. In summary, when the material and the loading are such that $\ell_c \ll W$, the condition $\ell \ll W$ alone is not sufficient to prevent broadening.

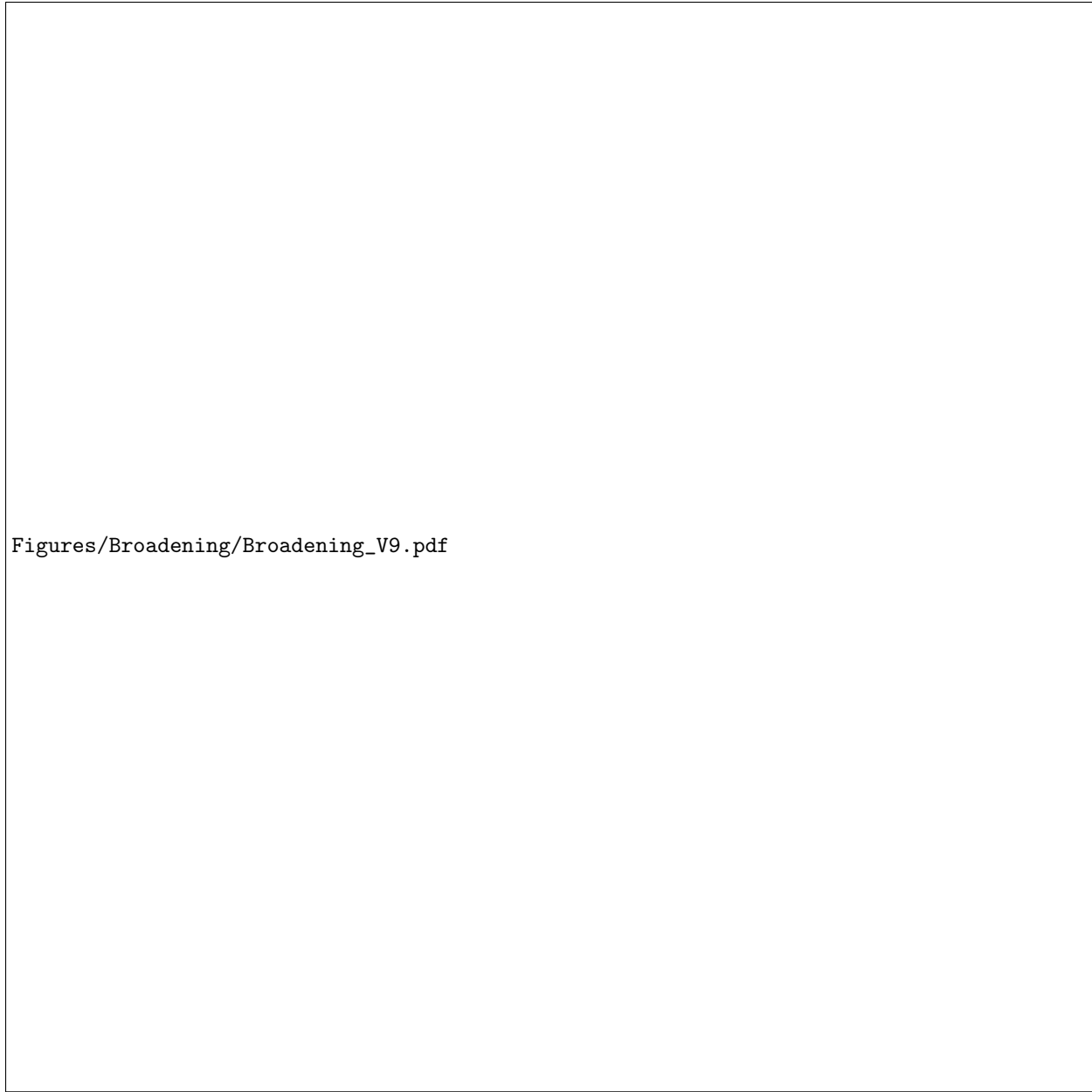
Our preliminary research also has the following important consequence. In view of broadening, current RVFT cannot be used as the basis for developing practical investigative tools. As per a Γ convergence [?]



Figures/VRF/Figure1_box_ver9.pdf

Figure 6: Comparison of RVFT predictions with LEFM and experiments. (a) Edge-notched geometry subjected to a far-field stress σ^∞ . The dimensionless stress at which the crack initiates σ_{cr}^∞/E^* as a function of dimensionless variables, g_c/E^*b and a/b obtained from the analytical solution. For different values of g_c/E^*b , the markers lie close to the reference line shown in gray within an error of 5%. (b) Comparison of RVFT predictions with an edge notch three-point bending test in which the sample has three holes drilled in it. (i) The experimentally measured crack path from [?]. (ii) Contour of the damage field d , where $d = 1$ is indicated by red contour level signifying the location of the crack. (iii) Comparison of the measured crack path and the RVFT predictions using the crack angle, θ shown in (ii).

{f:VFTvalidat



Figures/Broadening/Broadening_V9.pdf

Figure 7: Example simulations demonstrating the problem of crack broadening. (a) Experiment geometry and problem parameters. Only the lower half of the plate in the \hat{e}_2 direction is shown since $d \approx 0$ in the upper half for (a)–(c). The notch is not explicitly incorporated as part of the plate's geometry but rather is represented as a small region where $d = 1$, as shown in the inset. (b) The plate in (a) is loaded in uniaxial tension by displacing the boundaries marked in gray in the $\pm\hat{e}_1$ direction. A crack (the red contour level) propagates from the notch in the \hat{e}_2 direction until the plate is cleaved into two pieces. The crack's thickness is roughly equal to ℓ . (c) The plate in (a) is loaded in uniaxial tension parallel to the notch direction by displacing the boundaries marked in gray in the $\pm\hat{e}_2$ direction. Damage progresses from the notch in the $\pm\hat{e}_1$ directions until there is a region of completely disintegrated material (i.e., $d \approx 1$) spanning the entire width of the plate. The thickness of this region is much larger than ℓ . (d) A 2D strip with infinite length in the \hat{e}_2 direction stretched parallel to a crack (shown in red) along its length. (g) The variation of the damage, d , over the half-width of the 2D cracked strip shown in (d). The variable $\xi = x/W$, and x is the Cartesian coordinate in the \hat{e}_1 direction shown in (d).

{f:broadening}

proof given in [? ?] the solution of the variational problem (1) is physically meaningful (i.e., it corresponds to brittle fracture) only in the limit $\ell \rightarrow 0$. From a practical perspective, the computational cost grows inversely with ℓ . Therefore, one would like to use as large an ℓ as possible. However, the proof does not tell us what the largest value for ℓ is at which the results can still be meaningful. Our analysis answers this question

by stating that ℓ should at least be smaller than $\min\{W, \ell_c\}$. This might suggest that the solution to the broadening problem is straightforward—simply make ℓ smaller than both W and ℓ_c . However, this is much easier said than done. For most practical applications, the value for ℓ_c is so small that using ℓ values smaller than ℓ_c is impractical. For example, $\ell_c \approx 10 \text{ nm}$ for silicon. In 2D, even a $1 \mu\text{m}$ square specimen would require us solving one million equations. Of course, with recent advances in parallelization and computational power it is routinely possible to solve such large systems of equations on computer clusters. However, pursuing the project's research objective requires us to run a RVFT simulation repeatedly to study the effect of different architectural motifs on the manner in which crack patterns evolve and affect the toughness. Currently, solving 0.3 million equations takes us 56 hours of CPU time when solving them in parallel on 16 CPU cores. Thus, in summary, our analysis shows that broadening is a major problem, and because of it computational simulations based on the current RVFT cannot be used as practical investigative tools.

{sec:Startegy}

4 Research plan: aims and tasks

{s:aims}

We will pursue the project's overarching research objective by pursuing the following two specific aims and carrying out their associated tasks.

Aim 1 (A1): Develop a new variational fracture theory and computational framework that are capable of robustly simulating crack topology changes (crack branching, merging, etc.) in composites with complex, 3D architectures and heterogeneities.

Task A1.T1 *Develop a new RVFT that will be free of the problem of crack broadening. We term this new RVFT the anisotropic RVFT or aRVFT.*

Task A1.T2 *Develop new computational tools through implementing nonlinear finite element techniques to numerically solve the aRVFT.*

Task A1.T3 Simulate well studied linear elastic fracture mechanics problems and well known experimental fracture tests using the computational tools developed in A1.T2.

Aim 2 (A2): If the new RVFT is to function as an investigative tool for identifying the key architectural features, then it is important that it is able to reproduce the salient features of the experimentally observed failure responses of composites. We will use a computational implementation of the new RVFT to simulate the failure of a model SB—spicules from the marine sponge *Euplectella aspergillum*. We will then compare the results from the RVFT simulation with measurements from fracture tests conducted on the spicules and evaluate whether the RVFT was able to capture the spicules' failure behavior.

Task A2.T1 *Build an aRVFT computational model for the spicule.* In order to build an aRVFT model of a spicule we must first characterize the spicule's architecture and measure the mechanical properties of its constituent material and the interfaces within it.

Task A2.T2 *Characterize the spicules' failure behavior.* Perform three point bending tests on notched spicules and measure their load-displacement responses.

Task A2.T3 *Compare the measurements to the aRVFT tool's predictions.* Use the load-displacement responses as well as the work of fracture, or the total energy dissipated during failure, as metrics for comparison.

4.1 A1, Develop a new variational fracture theory and computational framework that are capable of robustly simulating crack topology changes

{s:A1}

Through our preliminary research we have developed a promising strategy to eliminate the problem of broadening. The primary issue in the current RVFT is that stiffness is uniformly degraded in all directions as d increases. We illustrate this situation schematically in Figure 7 (e), where bonds both perpendicular and parallel to the crack are broken. Physically, however, it is only necessary that the bonds perpendicular to the crack are broken, as illustrated, e.g., in Figure 7 (f). We found that the RVFT artificially degrading the parallel bonds is the source of the broadening effect. Therefore, we will solve the problem of broadening

by developing a new RVFT in which the parallel bonds remain intact. Due to the anisotropic breaking of bonds, we refer to our new RVFT as anisotropic RVFT, or aRVFT. We will begin the development of aRVFT by introducing in it information about the crack orientation and using that information to degrade only the bonds that are normal to the crack surface. Specifically, we will begin by making the strain energy term in (1) have the more general form $\int_{\mathcal{B}_0} \Psi(\mathbf{X}, \mathbf{F}, \hat{\mathbf{D}}, d) d\Omega$, where $\hat{\mathbf{D}}$ is a unit vector containing information about the orientation of the crack. If $d = 1$ at some \mathbf{X}_c and there is a single crack containing \mathbf{X}_c , then $\hat{\mathbf{D}}(\mathbf{X}_c)$ is interpreted as a direction that is normal to that crack at \mathbf{X}_c . Using $\hat{\mathbf{D}}$ we will construct Ψ such that the stiffness is only degraded in the direction normal to the crack. Our preliminary calculations show that this strategy is promising for resolving the problem of broadening. We present an example calculation below.

A1.T1: Develop a new RVFT that will be free of the problem of crack broadening The construction of Ψ may appear challenging. However, it can be simplified by making use of the fact that any proposed Ψ has to satisfy the fundamental principles of material behavior and mechanics. For example, we will reduce the allowable forms of Ψ by requiring that it obey the principle of material frame indifference, and respect the symmetries of the material. For instance, we found that for an isotropic material Ψ satisfies these conditions if it has the reduced form $\Psi(\mathbf{X}, \hat{\mathbf{D}} \cdot \mathbf{A}(\mathbf{U})\hat{\mathbf{D}}, \lambda_1, \lambda_2, \lambda_3)$, where \mathbf{U} is the positive square root of \mathbf{C} , $(\lambda_1, \lambda_2, \lambda_3)$ are the eigenvalues of \mathbf{U} , and the tensor valued function $\mathbf{A}(\mathbf{U})$ satisfies the condition $\mathbf{A}(\mathbf{Q}\mathbf{U}\mathbf{Q}^T) = \mathbf{Q}\mathbf{A}(\mathbf{U})\mathbf{Q}^T$. For example, in 2D consider $\Psi_d^{NH} = \mu/2((\lambda_1^2 + \lambda_2^2 - 2) - d(a_1^2\lambda_1^2 + a_2^2\lambda_2^2 - 1))$, where a_1, a_2 are the components of $\hat{\mathbf{D}}$ in the eigenvector directions of \mathbf{U} . This strain energy density function is a specialization of the reduced form for the case $\mathbf{A}(\mathbf{U}) = \mathbf{U}^2$. When $d = 0$ everywhere then it reduces to the classical incompressible neo-Hookean material model.

If we re-solve the 2D cracked strip problem (see Figure 7 (d)) using Ψ_d^{NH} instead of the previously used $(1-d)^2(\mu/2)(\lambda_1^2 + \lambda_2^2 - 2)$, then we find that if $\ell \ll W$ then at distances of the order of ℓ away from the pre-existing crack $d(\xi) < 2e^{-1/\ell} + O(e^{-2/\ell}) \approx 0$ irrespective of the amount of stretch λ_2 or the value of μ . Thus, with the new Ψ_d^{NH} the broadening effect has vanished. These are fascinating results. They give us confidence that we are looking in the right direction for solving our research problems and also give us a glimpse of the highly valuable advances that are possible by pursuing the outlined research to its conclusion.

As the logical next step, we will ensure that broadening had indeed been eliminated through using Ψ_d^{NH} by analytically solving and analyzing other idealized test problems of the type shown in Fig. 7 (d). In those test problems we will consider more complex stress states in both 2D and 3D. Using Ψ_d^{NH} as guidance, we will derive a family of degraded strain energy density functions that too similarly eliminate broadening and additionally apply to 3D situations, compressible regimes, and heterogenous solids. For this new family of energy density functions, we will derive the nonlinear partial differential equation (PDE) that d is required to satisfy from it being the solution to the variational problem (1). We will derive different versions of this PDE that correspond to progressively more complex situations. For example, we will move from small to finite deformations, homogenous to heterogenous solids, 2 to 3D, and quasi-statics to dynamics.

A1.T2: Numerically implement aRVFT We will numerically implement the new aRVFT using the same finite element techniques and nonlinear solver algorithms that we used for producing the preliminary results shown in Figure 4, 6, and 10. The numerical implementation will move from simple versions of the aRVFT to progressively more complex versions. For example, we will first implement a 2D version and then a 3D version. Similarly, we will first implement the aRVFT for the case of small deformations and then later for finite deformations. For simulating quasistatic loading programs we will use the nonlinear solver algorithms used in [?]. For simulating dynamics we will use the time integration algorithms used in [?]. In the final stages we will implement the augmentations used by Miehe [?] to constrain the damage variable at all material materials from ever decreasing with either load-step (in quasistatic simulations) or time (in dynamics simulations). We will use the techniques described in [?] to avoid the spurious effect of the damage variable growing when the stress state is purely compressive.

A1.T3: Simulate well studied linear elastic fracture mechanics problems and well known experimental fracture tests using the computational tools developed in A1.T2. We will simulate the fracture mechanics problems and experimental tests shown in Figs. 4, 6, and 10 using the computational tools developed via A1.T2. We will use these simulations to ensure that broadening has indeed been eliminated

in the newly developed computational tools, and that the simulations performed using the newly developed computational tools are indeed more computationally affordable than those based on the RVFT.

4.2 A2, Evaluate the predictive potential of the aRVFT through experimental comparison

{s:A2}

The aRVFT-based computational tools will be free of the problem of broadening and therefore will be able to model the evolution of complex fracture patterns in realistic models of composites with complex architectures, namely SBs. The goal of developing the aRVFT is to use it for performing accurate and robust virtual experiments on ceramic composites. However, to realize this goal it is important that the aRVFT tools are able to correctly capture the salient characteristics of a composite's failure behavior. We will evaluate the predictive capability of the developed aRVFT tools by comparing their results with measurements from fracture tests conducted on a model SB with 3D architecture.

We will use the skeletal elements of the marine sponge *Euplectella aspergillum*, called spicules, as the model SB in our evaluation [? ?]. The *E. aspergillum* spicules are hair-like fibers that are roughly 10 cm long and 50 μm in diameter and are composed primarily of silica. They have a tubular, tree-ring type architecture (see Figure 8 (a)) and our preliminary mechanical tests suggest that the interfaces between adjacent silica cylinders are weak. The PI has considerable experience studying structure-property connections in spicules [? ? ?]. However, the primary reason for selecting *E. aspergillum* spicules over other SBs, such as shell or bone, is that their architecture has a good balance between mathematical regularity and complexity. Owing to their axisymmetry, the *E. aspergillum* spicules can be described using less than 30 parameters. This will allow us to build CAD models of the spicules and complete our evaluation within the allocated time period of the project. Furthermore, our preliminary mechanical tests show that the *E. aspergillum* spicules' failure response is considerably different from that of spicules from a related species that lack the tree-ring architecture [?]. This implies that there are interesting architecture-created toughening mechanisms operating in *E. aspergillum* spicules.

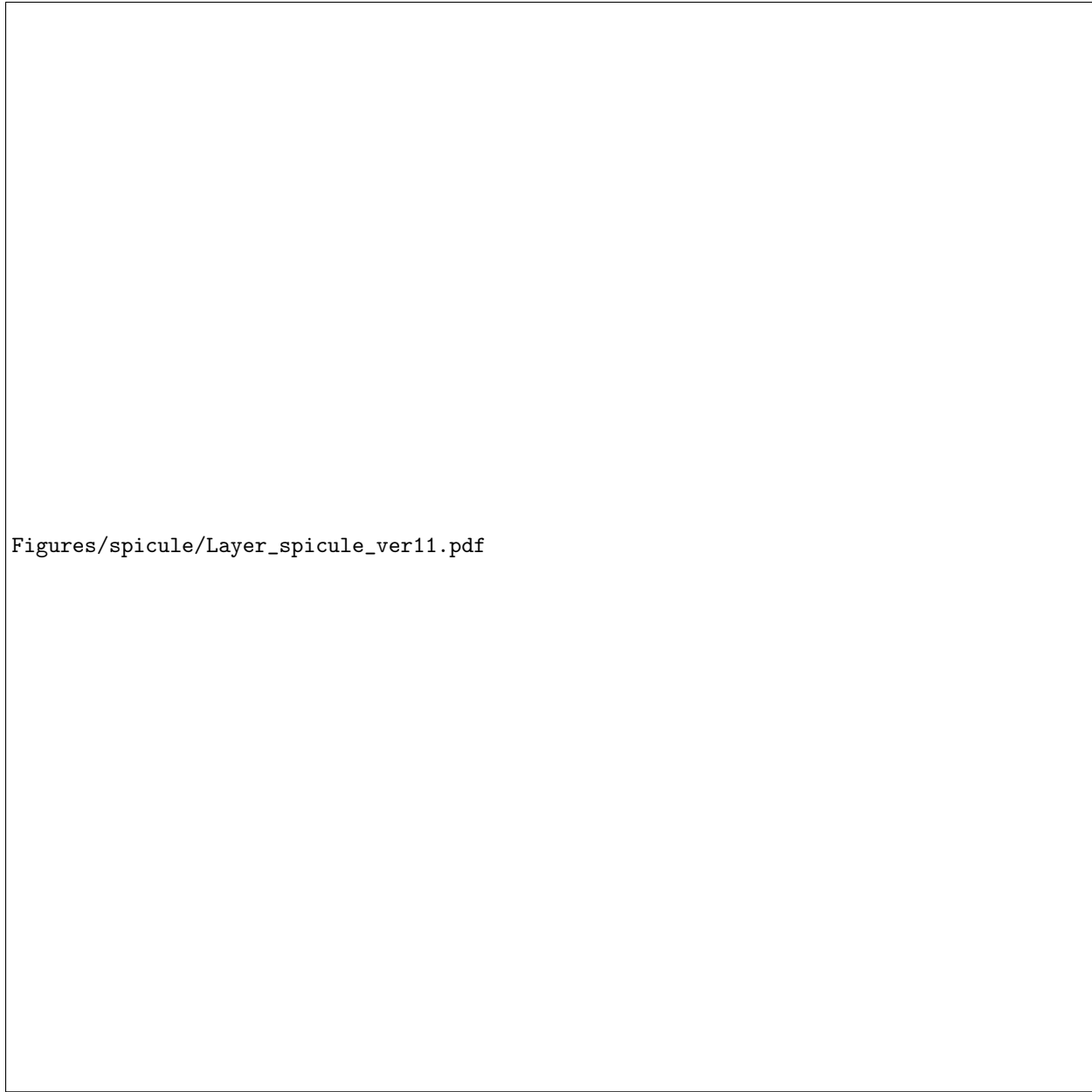
A2.T1: Build an aRVFT computational model for the spicule To build an aRVFT computational model of the spicule we need the following information: spicule architectural parameters, elastic and fracture toughness properties of the spicule's silica, and fracture toughness of the spicule's interfaces. This data will be collected by completing the following subtasks:

T1.i) Architecture measurements. The PI has used SEM imaging to measure the silica cylinder thicknesses in the *E. aspergillum* spicules as reported in [?]. We will measure the spicule radius, core radius, and silica cylinder thicknesses using the same procedures used in [?] in all spicules that we test in Task.2.

T1.ii) Measure fracture toughness and elastic modulus of the spicule's biogenic silica. Although the *E. aspergillum* spicules are predominantly composed of silica, it has been shown that many spicules from other sponge species possess a proteinaceous scaffold within their silica [? ?]. Therefore, we will measure the elastic modulus and toughness of the *E. aspergillum* spicules' silica using nanoindentation. The toughness properties of the silica cylinders in the spicules of the sponge *Monorhaphis chuni* have previously been measured using nanoindentation [? ?]. We will use the same experimental protocol in our work. The spicule's core is roughly 20 μm in diameter, which is a sufficient area for performing the nanoindentation tests. We will compute the silica's toughness using the classic Lawn-Evans-Marshall model [? ?]. Nanoindentation will also be used for measuring the silica's reduced elastic modulus, E^* . For that purpose we will follow the procedure described in [?]. The PI has previous experience measuring mechanical properties using nanoindentation [? ?].

T1.iii) Measure the fracture toughness of spicules' interfaces. Since the spicules' silica cylinders are both thin and brittle, measuring the fracture toughness, g_I , of the weak interfaces between them is a challenging task. Motivated by the classical fiber push-out test [?], which is used to measure interface toughness in fiber reinforced composites, we have designed the following "cylinder push-out" test for measuring g_I .

One broken spicule segment from each bending test (see Task.2) will be embedded in epoxy and cross-sectioned using a diamond saw to create a 1–3 mm thick slab (see Figure 8 (e)). The exposed spicule cross-section will first be polished, and then a blunt diamond indenter will be used to push against the core. On the opposite side of the slab, all silica cylinders will be mechanically supported (see Figure 8 (e)). This configuration will freeze the relative motion of all weak interfaces except the first one between the core and



Figures/spicule/Layer_spicule_ver11.pdf

Figure 8: Measurement of the mechanical properties and behavior of spicules. (a) A SEM image of a *E. aspergillum* spicule's cross-section showing its layered architecture. The scale bar measure $10 \mu\text{m}$. (b) The three-point bending configuration used for the fracture tests described in A2.T2. The spicule is encastered at both ends with epoxy. A wedge-like indenter applies a force F midway along the spicule's length perpendicular to its axis. (c) SEM micrograph of a notch cut in a spicule using FIB milling. The scale bar measures 500 nm. (d) The load-displacement response of a notched spicule (shown schematically in (b)). (e) Configuration of the the proposed cylinder push-out test. A spicule is embedded in epoxy, and cross-sectioned along the orange planes. The silica cylinders from the cross-section are mechanically supported from below and the core is pushed from above (shown in gray). The light blue lines indicate the interfaces between silica cylinders and between the first cylinder and the core. The initial interface crack with length l_d is marked. (f) A typical load-displacement response obtained from a fiber push-out test (data obtained from [?]). {f:exp}

its adjacent silica cylinder. Thus, the core and the silica cylinders are analogous to the fiber and matrix, respectively, in the fiber push-out test [?].

We will adapt the mechanical testing system, which we use to perform the bending tests (A2.T2), to perform the cylinder push-out test. During the test we will measure the applied force and indenter displacement. We have made preliminary estimates of the force and displacement ranges needed for this test and found

that our modified testing system will be able to perform the cylinder push-out test with 50 nm displacement resolution and 4 μN force resolution.

A typical load-displacement curve from a fiber push-out test performed on a silicon carbide fiber reinforced composite is shown in Figure 8 (f). Initially, the applied force increases linearly with indenter displacement. The abrupt drop in force from P_d to P'_d corresponds to the formation of a crack along the fiber-matrix interface shown schematically in Figure 8 (e). Upon further loading, the applied force again increases until it reaches P_i , at which point the crack begins to propagate along the length of the fiber. If the length of the crack, l_d , at P'_d is large compared to the core radius, r_0 , then the initiation force, P_i , is related to g_I as $P_i = 2\pi\sqrt{r_0^3 g_I E^*}$ [? ? ?]. Knowing E^* (from T.1.ii), and r_0 (from T.1.i), we will compute g_I by measuring P_i in the cylinder push-out test. However, after the test is completed we must verify that $l_d \gg r_0$. We can compute l_d by measuring the stiffness from the force-displacement response before and after crack nucleation, and choosing l_d in a finite element model to match this stiffness ratio. If l_d is not much larger than r_0 , then we will numerically compute the energy release rate for the cylinder push-out test using a finite element model in order to obtain g_I [?].

A2.T2: Characterize the spicules' failure behavior We will characterize the spicules' failure behavior by measuring the load-displacement response of a notched spicule in a three-point bending fracture test. The PI has designed and built a mechanical testing system that is capable of performing the fracture tests with 200 nm displacement resolution and 20 μN force resolution [? ?]. The system's design is based on that of an Atomic Force Microscope (AFM). The PI has considerable experience using the AFM for performing mechanical tests [? ?] and has already performed three-point bending tests on spicules without notches using this custom-built system [? ? ?]. In the proposed tests, we will cut notches in the spicules in order to match the initial damaged state of the spicules in the experiments with the simulations. Through our preliminary research we were able to successfully create 5–25 μm long notches with a sharpness of approximately 100 nm using focused ion beam milling (see Figure 8 (c)).

Preliminary results from a bending fracture test performed on a notched spicule are shown in Figure 8 (d). The applied force, F , and load-line displacement, w_0 , are measured as the spicule is loaded in the configuration shown in Figure 8 (b). The spicule is first loaded (yellow points) until a crack emanating from the notch root propagates completely across the spicule's cross-section. The spicule is then unloaded (blue points), and the area between the loading and unloading branches (shown in purple) constitutes the total energy dissipated by the fracture process.

A2.T3: Compare the measurements to the aRVFT tool's predictions We have designed the experiments and simulations so that the geometry, internal architecture, initial damage condition, and material properties match as closely as possible. Thus, we can characterize the aRVFT's predictive capability by whether it is able to reproduce the measured load-displacement curves. Based on statistics from our initial un-notched bending measurements, we plan on testing 60 spicules harvested from four different *E. aspergillum* skeletons.

Table 2: Project timeline

Task\Year	1	2	3
A1	T1	T2	T3
A2	T1.i, T2	T1.ii	T1.iii, T3

{t:timeline}

5 Broader impacts of the proposed work

Collaboration with the Sci-Toons initiative The Science Cartoons (Sci-Toons) initiative is a new strategy for communicating scientific research and concepts to a broad audience via storytelling, animation, high-quality multimedia and art. The initiative, part of broader impacts and education activities at Brown University's Science Center, engages STEM students, non-STEM students and faculty to create science animation videos that conceptualize and communicate science in an engaging and compelling manner to a broad range of audiences. The PI and his students will collaborate with the SciToons Creation Group (SCG), led by Dr. Oludurotimi Adetunji, Associate Dean for Undergraduate Research and Inclusive Sci-

{s:broaderimp}

ence; and Executive Producer of the Brown University SciToons Initiative. The SCG consists of both STEM and non-STEM students, STEM domain content experts, voice over artists and animators.

The Sci-Toons program's broader impacts goal of fostering greater understanding and appreciation of science in the general public is advanced by meshing communication and science, skills and interests of STEM and non-STEM majors. Four students, the PI and Dr. Adetunji are currently collaborating to produce a Sci-Toon animation that, through "jargon-free" language and storytelling, communicates the importance and impact of the results from the PI's recent publication [?] to a non-scientific audience. As part of the proposed project, the PI, in collaboration with SCG, will create one video per academic year for the next five years. The collaboration through this proposal will begin in Fall 2018. The videos will focus on the latest results from the research wing of the project. They will end by highlighting that the vast majority of the nature's designs are still unknown, and we will try to excite the viewers about the immense possibilities that the discovery of such designs would create for science and engineering. Funds to support the PI's future collaboration with the Sci-Toons initiative are requested as part of the budget (see Budget Justification). *Evaluation:* The viewing impacts of Sci-Toons videos are gauged by monitoring the number and geographic distribution of views the videos generate using google analytics data. Prior Sci-Toons videos have been viewed in over 180 countries. Examples of completed Sci-Toons can be viewed on the Sci-Toons' YouTube channel.

In addition to the Sci-Toons YouTube channel and a dedicated website, the Sci-Toons videos are distributed via a variety of social media platforms, such as Twitter (@Sci_Toons) and Facebook. The Sci-Toons videos will also be posted on the PI's lab website. The website will be set up so that viewers can post comments and questions about the videos. The PI and his students will host a monthly virtual discussion group on Google Hangouts and address the posted comments and questions live. The PI will use the Sci-Toons videos in the undergraduate courses he teaches at Brown, such as Advanced Engineering Mechanics (ENGN 1370) and Advanced Engineering Optimization (ENGN 1950), which share the elements of solid and structural mechanics, and optimization principles with the topics that will be highlighted in the videos. The PI will also encourage his colleagues at Brown and other universities to use the videos in introductory engineering courses and in courses related to mechanics and optimization. *Evaluation:* The videos' impact and utility in the classroom will be gauged by using the end of course student feedback form.

Collaboration with SPIRA SPIRA is a four week camp hosted at Brown every summer for high school age girls to explore engineering. For the past three years, the PI and his students have been collaborating with SPIRA in order to encourage young women to pursue education in STEM fields by exposing them to interesting applications of engineering. The camp is free to those who attend and often attracts students from underrepresented minorities. Over the course of the proposed project, every summer, the PI and the students associated with the project will design and organize talks, workshops and competitions for the SPIRA participants. These activities will be tailored to make the participants aware of the wide range of exciting opportunities that are only recently becoming available to engineers, and through this awareness attract them to science and engineering. *Talks:* Some of the past talks have been "Better materials through micro-scale mechanical design" and "Bio-inspired engineering: why should we listen to nature." These talks were focused on the importance of bio-inspired materials to the future of mechanical engineering. Future talks will have a similar focus. The new results from the research component of the project will be used to enhance the quality of the talks. Following the talk, the students will be given a tour of PI's lab during which the presented research will be further explained using physical examples and practical demonstrations. *Lab tour and workshop:* During the lab tour, the PI and his students will also explain the operating principles behind the different lab equipment. Last year's workshop was titled, "Hidden genius: a closer look at nature's architecture." In it, the participants examined spicules from the *E. aspergillum* sponge as well as other biomaterials. Pictures from last year's lab tour and workshop are shown in Figure ???. The first workshop that will be held as part of the project is tentatively titled, "Engineering Principles in Nature". In it, the PI's team and the participants will discuss the size, form, and function relationships in SBs, such as mammalian bones, eggshells, gecko's feet and the venus fly trap. *Competition:* The competitions will give the participants an opportunity to learn through hands-on practice and experimentation. A competition under development for this project's SPIRA activities is tentatively titled "Soft landing: better materials for tomorrow's helmets and cars". In the competition the participants will be asked to construct a structure for cushioning the fall of a dropped egg by taking inspiration from nature. The student teams will be supplied

with various materials and given access to the microscope in the PI's lab. Funds to organize this new competition in collaboration with SPIRA are requested as part of the budget (see Budget Justification). **Evaluation:** The effectiveness of the planned SPIRA lectures, tutorials, and competitions will be gauged using exit interviews. The students' feedback will also be solicited by encouraging them to post comments and suggestions on the SPIRA section of the PI's website.

6 Results from prior NSF support

CMMI-1562656: "Emergence of New Properties at the Large-Scale on Elastic Surfaces due to Small-Scale Adhesion and Waviness," \$375,000, 03/01/2016 – 02/28/2019. **Intellectual merit** The objective of this research is to understand how contact interactions between two surfaces at the micro-scale manifest as friction-like behavior at the macro-scale. Specifically, we relate friction at the macro-scale to dissipative mechanisms acting at the micro-scale that are activated by both adhesion and surface roughness. Through a synergistic combination of theoretical analysis, computer modeling, and experiments we will develop a rigorous mechanical theory governing the relationship between friction, adhesion, and surface roughness. A better understanding of this relationship could lead to advances in pick-and-place technology, MEMS, and biomimetic climbing robots. Four peer reviewed journal articles have been produced under this award so far, and three others are currently in preparation. Additionally, results from these articles have been disseminated through six conference presentations. As per the Data Management Plan for this award, computer code, experimental data, and theoretical results are made available through the Dropbox cloud storage system. **Broader impacts** Five graduate students (Wenqiang Fang, Weilin Deng, Michael Monn, Jarod Ferreira, Jianzhe Yang), and one undergraduate student (Christopher Owen-Elia) have worked on projects supported by this award. Two masters theses titled "Adhesive contact experiments with non-linear model fitting" and "Deep indentation contact experiments with nonlinear model fitting" have been completed by Jarod Ferreira and Jianzhe Yang, respectively, under the supervision of the PI. Finally, the PI has worked with the SciToons initiative at Brown University to create the first of a series of animated videos with a focus on bio-inspired engineering. The PI's collaboration with SciToons will be used to communicate research results to the STEM-interested public.

{s:priorfund}

A Appendix

A.1 Elaboration of the suitability of CZM and XFEM for the prusing the research objectives of this project

{sec:CZM_XFEM}

Cohesive zone (CZ) methods have proven to be very significant for modeling interfacial fracture. There are several versions of CZ methods discussed in literature. Most of those methods can be put into two primary classes. The first class is roughly based on the numeric implementation of Hillerborg et al.[?] while the second class is based on the ideas of Xu and Needleman [?], and Camacho and Ortiz [?]. Both classes are based on the work of Dugdale [?] and Barenblatt [?] and built atop of classical finite elements techniques. In that crack growth is modeled by allowing adjoining finite element pairs to separate along their shared boundary. As the elements separate, tractions are applied on the separating faces of the elements as per a pre-assigned traction-separation law. The shape and parameters in the traction separation law are chosen to model different types of damage behavior (ductile, quasi-brittle, etc.). This idea is made numerically feasible by incorporating what are termed *cohesive zone (or interface) elements* between the shared boundaries of adjoining finite element pairs. The primary difference between the two classes of CZ methods is in the selection of the finite element boundaries at which the CZ elements are included.

In the classical version of the CZ method, given by Hillerborg et al., the CZ elements are only placed along finite element boundaries which are known/expected to be close to the final crack path. Thus, the application of the classical CZM is predicated upon having some *a priori* knowledge of the crack path. However, the success of the proposed research program hinges on developing and leveraging the ability to predict the evolution of complicated crack paths of which we have no or very little *a priori* knowledge. Consequently, classical CZ methods are not suitable for the proposed research project.

In the generalized version presented by Xu and Needleman the CZ elements are placed between all shared boundaries of the finite elements. This enables the simulation of crack propagation without requiring any *a priori* knowledge of the crack path. This generalized version is also capable of modeling the evolution of

complicated crack paths. However, based on our study of the computational mechanics literature and the preliminary research that we undertook for planning the proposed project we found that the generalized CZ method is not very accurate in reproducing experimentally observed crack paths [? ? ?]. For example, Figure 9 shows a comparison between experimentally observed crack paths and those that were computationally predicted using the generalized CZ method. As can be seen by comparing Figure 9(a) with either (b) or (c), the generalized CZ method predicted cracks paths are quite different from the experimentally observed ones. Furthermore, as can be seen from Figs. 9(b)–(c), the generalized CZ method predicted crack paths are *mesh dependent*. That is, they depend on the size and structure of the finite element mesh employed.

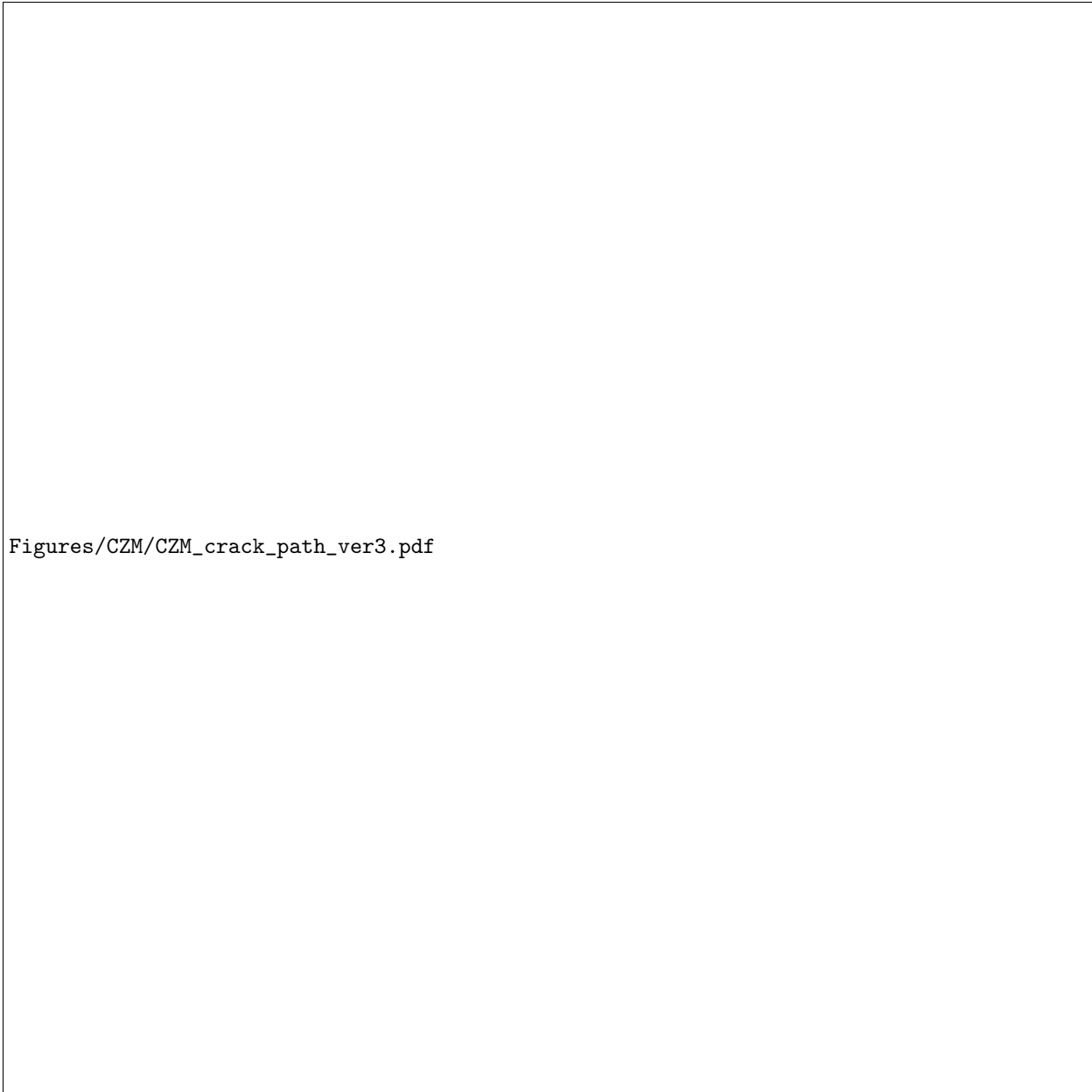
The inaccuracy and mesh sensitivity of the generalized CZ method is widely discussed in literature [? ? ? ?]. We do not have any ideas as how to remedy the generalized CZ method's poor accuracy and high mesh sensitivity. Therefore, we decided not to select it for further development for the purpose of our pursuing the project's overarching research objective.

Extended Finite Element methods (XFEM). The XFEM is a remarkable method. It has been used to simulate quasi-static crack growth in both 2D [? ? ?] and 3D [? ? ?], and dynamic crack growth in 2D [? ?]. It is currently widely used to predict crack paths [? ? ?] and is even a feature in the commercial finite element software package Abaqus [?]. It was introduced by Belytschko and Black [?] for modeling cracks in solids without the need for remeshing. The numerical ideas underlying XFEM are based on the partition of unity concept of Melenk and Babuška [?]. Currently, there are several versions of the XFEM discussed in its literature. So, it is not unlikely that our comments will not apply to all of them. Also, we have sincerely tried not to cherry pick which features of the XFEM we discuss so as not to give an unfair appraisal of its capabilities.

Like CZ methods, the XFEM too is built atop of finite elements methods. In standard finite element method (FEM), the displacements, strains, etc. are approximated as linear combinations of a select set of functions called the *basis functions*. Choosing a finite element mesh and the finite element type(s) (linear tetrahedron, etc.) in a problem is tantamount to choosing the set of basis functions. In standard FEMs, the basis functions are usually continuous or smooth. The coefficients of the basis functions in the linear combinations are related to the degrees of freedom at the finite element nodes. In simulations based on standard FEMs, the set of basis functions remains fixed during the simulations. The ingenuity of the XFEM lies in the following two modifications: (i) In addition to the usual continuous/smooth basis functions, discontinuous and irregular basis functions are allowed in the set of basis functions. This process is called *enrichment*. The choice of these discontinuous/irregular basis functions is based on the asymptotic solutions of fracture problems in the linear theory of elasticity and the total deformation theory of plasticity. These new basis functions enable the XFEM to capture the discontinuities across the crack's faces and the singular behavior at its tip. (ii) The crack growth is modeled by allowing the set of basis functions to change as the crack grows.

Despite its tremendous utility, the XFEM is not suitable for pursuing the objectives of the current proposal. This is because the XFEM in its classical form cannot be used to model topology changes (see, e.g., Figure 3). That is, it cannot be used to capture phenomena such as the merging of two (or more) cracks to form a single crack (Figure 3(a).i–ii), the splitting of a crack into two (or more) daughter branches (Figure 3(b).i–iii), and the nucleation of new cracks (Figure 3(c).i–iii). This is not to say that XFEM cannot apply to a crack that contains one or more branches. Indeed, special enrichment functions have been developed through which XFEM can yield the displacements, stresses, etc. in problems that contain a crack with multiple branches [? ?]. However, even with those special enrichments the XFEM on its own—i.e., without any modeler input during the simulation, or *a priori* knowledge about any forthcoming topology changes—will not be able to predict whether or not a crack will split into multiple branches, and if does split, how many branches it will split into.

Topology changes are not very common in quasi-static crack growth problems in homogenous materials. However, as we discussed in §1.2, topology changes are very common in heterogeneous materials, such as structural biomaterials. In fact, topology changes are a key feature of the mechanisms through which hypothesize that the structural biomaterials gain their remarkable toughness. It is possible to augment the XFEM with features from CZ methods [? ? ?], or using older failure theories, such as the *critical principle stress failure criteria*, to give XFEMs some capability for capturing topology changes. However, we are not

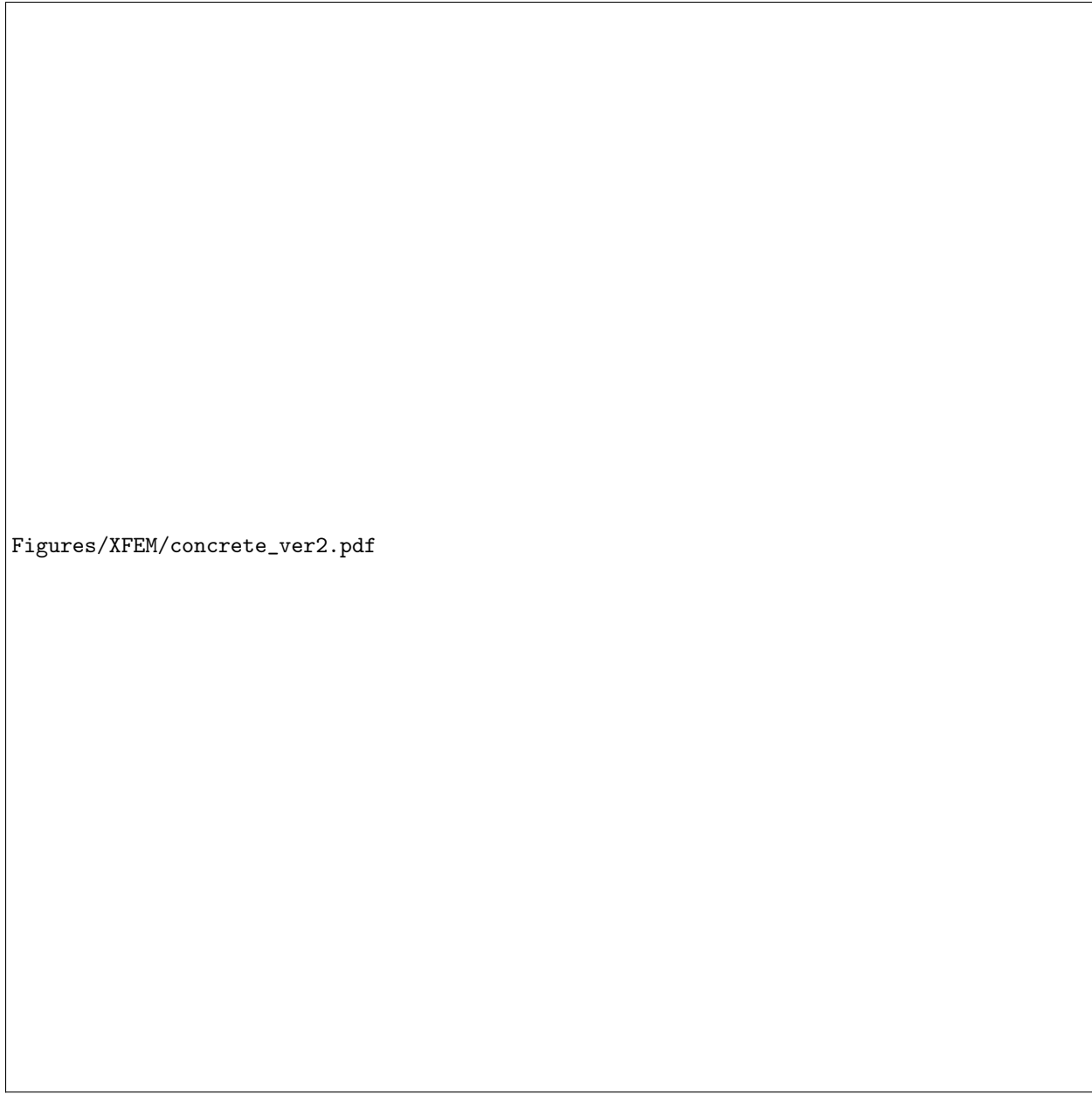


Figures/CZM/CZM_crack_path_ver3.pdf

Figure 9: Comparison between experimentally observed and computationally predicted crack paths. (a) shows the experimental crack paths observed in concrete specimens by Schlangen [?] and the corresponding experimental setup is shown in the inset, which is a single edge notch (SEN) shear load test. Each curve corresponds to a different specimen. (b) and (c) show the computationally predicted crack paths for a coarse and fine finite element mesh, respectively. These computational crack paths were predicted by Tijssens et al. [?] for the experiments shown in (a) using the generalized CZ method.

{f:czm}

aware of any rational/scientific theory that can guide such an augmentation. Without a systematic means to guide the augmentation, we are afraid that any such augmentations can only be heuristic or *ad-hoc* at best and therefore cannot be the primary agenda of a scientific project. The RVF theory, on the other hand, can readily model topology changes without any heuristic/*ad-hoc* augmentations, see Figure 10 and Figure ??, e.g. For these reasons, we decided not to select the XFEM for pursuing the project's research objective.



Figures/XFEM/concrete_ver2.pdf

Figure 10: Comparison between experimentally observed and computationally predicted crack paths. (a) shows a photograph of a failed concrete specimen. This is from the experiments reported by Gálvez *et al.* [?]. The specimen was prepared by cutting two notches, one on each of its left and right edges. The only loading on the specimen was on its top portion. That is, the region above the notches was loaded in compression. The specimen was observed to fail through the formation and propagation of two distinct crack systems. The first system (marked in red dashed lines) consists of two cracks, each of which emanate from a notch and grow a short distance into the bottom portion of the specimen. The second system (marked in yellow dash-dot lines) consists of a single crack that nucleates in the top portion of the specimen and propagates symmetrically towards the left and right. (b) shows the predictions of the RVFT. As can be seen, the RVFT captures both system 1 and 2 of the cracks formed. Its predicted shape and length of the system 1 cracks is also quite consistent with what is experimentally observed. Its predicted shape and length of the system 2 crack is slightly different from what is observed in experiments. We believe that this disparity is due to the incomplete knowledge we have about the specimen's materials properties and the experiment's loading program. (c) shows the predictions from the XFEM (as implemented in Abaqus). The XFEM method is able to capture the system 1 cracks. However, it completely misses the system 2 cracks. This is expected, since as we discuss in the text, XFEM on its own cannot readily capture topology changes, of which crack nucleation is a special case. Also, the XFEM predicted length of the system 1 cracks is substantially different from what is observed experimentally.

{f:xfem}